Numerical analysis of Masonry Spandrels with Shallow Arches

Sujith Mangalathu
Rose Programme, UME School, IUSS Pavia, Italy.
Ecole Polytechnique Fédérale de Lausanne (EPFL), Switzerland

Katrin Beyer
Ecole Polytechnique Fédérale de Lausanne (EPFL), Switzerland.

15 WCEE
LISBOA 2012

SUMMARY:
In unreinforced masonry (URM) walls the vertical piers are connected by horizontal spandrel elements. These spandrel elements considerably affect the global wall behavior when subjected to seismic loading. Modeling of masonry walls without fully understanding the effect of spandrels can lead to erroneous results. Despite the importance of spandrels, the coupling action of spandrels is often neglected in design codes mainly due to the scarcity of experimental data on masonry spandrels and the absence of proper mechanical models. For the realistic seismic design of new buildings and assessment of existing buildings, mechanical models for masonry spandrels are required. In this study, numerical investigations are carried out based on the simplified micro-modeling approach using the ATENA software package. In the simplified micro-model, each brick is modeled as a separate unit and the mortar joints are represented by contact elements. The results of the numerical analyses are verified against experimental data from masonry spandrel tests. It is found that the results from numerical studies are in good agreement with the experimental values. The numerical model is then used to conduct a parametric study on the peak strength of the masonry spandrels with shallow arches.

Keywords: *Unreinforced masonry, spandrel elements, simplified micro-modeling*

1. INTRODUCTION

In unreinforced masonry (URM) walls, the vertical piers are connected by horizontal elements called spandrels. Recent earthquakes (e.g., L'Aquila, 2009, Fig. 1) have shown that the spandrel elements are often the first elements to crack or fail in a URM building under seismic loading. In spite of its importance, the framing action of the spandrel elements is neglected and only the vertical pier elements are considered while calculating the strength and the stiffness of the URM walls (Beyer and Dazio, 2012). Various researchers (Magenes, 2000; Beyer and Dazio, 2011) have pointed out that the spandrel elements considerably affect the force-deformation characteristics of the URM walls. The main reasons for ignoring the contribution of masonry spandrels are the scarcity of experimental data on masonry spandrels under seismic loading and the resulting absence of validated mechanical models. Recent experiments (Gattesco *et al*. 2008; Beyer and Dazio, 2012) have revealed the force-deformation characteristics of masonry spandrels. The objective of the current study is to obtain deeper insights into the behavior of masonry spandrels by numerical modeling.

The numerical representation of masonry can be achieved either by micro-modeling, i.e., modeling the constituents separately, or by macro-modeling, i.e., modeling the structure as a continuum. In micro-modeling the units are represented by continuum elements and the joints are modeled by interface elements. Depending upon the level of accuracy and simplicity, micro-modeling can be classified into two modeling approaches – detailed micro-modeling and simplified micro-modeling. In detailed micro-modeling, joints are represented by mortar continuous elements and discontinuous interface elements, while in simplified micro-modeling, joints are represented by discontinuum elements (Lourenco, 1994).
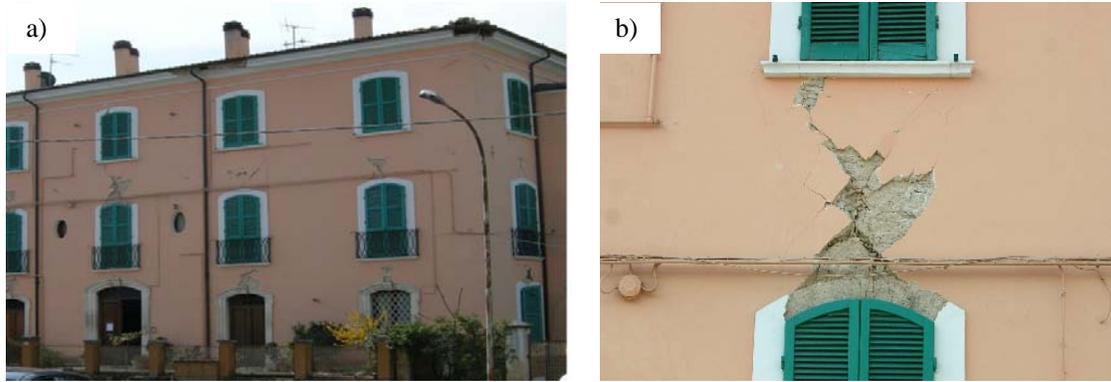
Figure 1. a. Old URM building during the L'Aquila earthquake on April 6th, 2009, showing spandrel failure; b. Detailed view of the spandrel failure (Beyer and Dazio, 2012), Photo b courtesy of A. Dazio

The macro-modeling approach (e.g., Gambarotta and Lagomarsino, 1997) models the whole structure as a continuum without any distinction between the units and joints. Macro-modeling is useful for studying the global response of the structure. Simplified micro-modeling is suitable for small structural elements as their responses can be closely represented using the knowledge of material properties. In the current study, simplified micro-modeling is adopted in order to capture the force-deformation characteristics of the masonry spandrels from the constituent properties. The current study focuses only on masonry spandrel elements with shallow arches and with constant axial load on the spandrel.

2. EXISTING PROVISIONS

FEMA 306 guidelines (ATC, 1998) and the Italian code OPCM 3431 (OPCM, 2005) are, to our knowledge, the only standards that propose equations for the strength of masonry spandrels. The current section provides a brief summary of the FEMA and OPCM models. For a detailed review of the various mechanical models for spandrels readers are referred to Beyer and Mangalathu (2012).

FEMA 306 addresses the peak and the residual strengths of masonry spandrels. The flexural capacity of the spandrel in FEMA 306 (Eq. 2.1, Table 1) is assumed to be derived from the shear stresses in joints between bricks that are pulled out due to the opening of a flexural crack at the interface between the pier and the spandrel. The peak shear strength capacity of the spandrel in FEMA 306 is based on the model by Turnsek and Cacovic (1970).

The Italian seismic design code OPCM 3431 (OPCM, 2005) provides guidelines for computing the shear and flexural capacities of spandrel elements in URM buildings (Table 1). It distinguishes between spandrel elements for which the axial forces are either known or unknown. If the axial force in the spandrel is known, the spandrels are treated like piers for the computation of shear strength associated with the flexural mechanism. If it is unknown, the flexural capacity of the spandrel is computed from a strut-and-tie mechanism by replacing the axial force in the spandrel, P_{sp} (Eq. 2.2) with the minimum of H_p and $0.4h_{sp}t_{sp}f_{hd}$, where H_p is the tensile strength of the horizontal tension elements such as steel ties or ring beams. The geometric parameters, height of the spandrel (h_{sp}) and thickness of spandrel (t_{sp}) are shown in Fig. 2 and f_{hd} is the design compressive strength of the masonry in the horizontal direction.

Like FEMA 306, OPCM 3431 adopts the shear capacity model by Turnsek and Cacovic (Eq. 2.5), if the axial force is known. If it is unknown, the shear capacity is computed using Eq. 2.3. OPCM 3431 also provides a shear capacity equation (Eq. 2.4) based on a sliding shear mechanism in the compression zone. It is, however, not clear whether the OPCM equations address the peak strength or the residual strength of the masonry spandrels.

Table 1 provides a summary of the FEMA and OPCM models. The geometric parameters l_{sp}, l_b, l_j, h_b and h_j in Table 1 are defined in Fig. 2. The variable f_{dt} in Table 1 is the diagonal tensile strength of the masonry, c the cohesion, μ the coefficient of friction, p_{sp} is the mean axial compressive stress in the spandrel ($p_{sp} = P_{sp}/h_{sp}t_{sp}$), and h_c the height of the compression zone.

Table 1. Summary of Equations for Predicting the Spandrel Strength (Beyer and Mangalathu, 2012)

FEMA	Flexure	$$V_{p,fl} = \frac{2}{l_{sp}} \cdot \frac{2}{3} h_{sp} \cdot f_{p,tot} \cdot \frac{h_{sp}}{4(h_j + h_b)} \quad ^{1)}$$ with $\quad f_{p,tot} = f_{p,bj} \cdot t_b \cdot \frac{l_b}{2} + f_{p,sj} \cdot \frac{l_b}{2} \cdot h_b \cdot (NB-1)$ $f_{p,bj} = c + 0.5 \cdot \sigma_{pier}$ where, NB = number of wythes	(2.1)
OPCM	Flexure	$$V_{fl} = P_{sp} \cdot \frac{h_{sp}}{l_{sp}} \left(1 - \frac{h_c}{h_{sp}}\right)$$	(2.2)
	Shear 1	$$V_s = h_{sp} t_{sp} c_{red} \quad \text{with} \quad c_{red} = c \frac{1}{1 + 2(h_j + h_b)/(l_b + l_j)}$$	(2.3)
	Shear 2	$$V_s = h_c t_{sp} \cdot c_{red} + 0.4 \cdot P_{sp} \quad \text{with} \quad h_c = \frac{P_{sp}}{0.85 f_{hd} t_{sp}}$$ and c_{red} as in Shear 1	(2.4)
Turnsek and Cacovic (1970)	Shear	$$V_{p,s} = f_{dt} \cdot h_{sp} \cdot t_{sp} \cdot \beta \cdot \sqrt{1 + \frac{P_{sp}}{f_{dt}}} \quad \text{with} \quad 0.67 \leq \frac{h_{sp}}{l_{sp}} \leq 1.00$$	(2.5)

[1] End moments are converted to a shear force assuming the spandrel is subjected to double bending
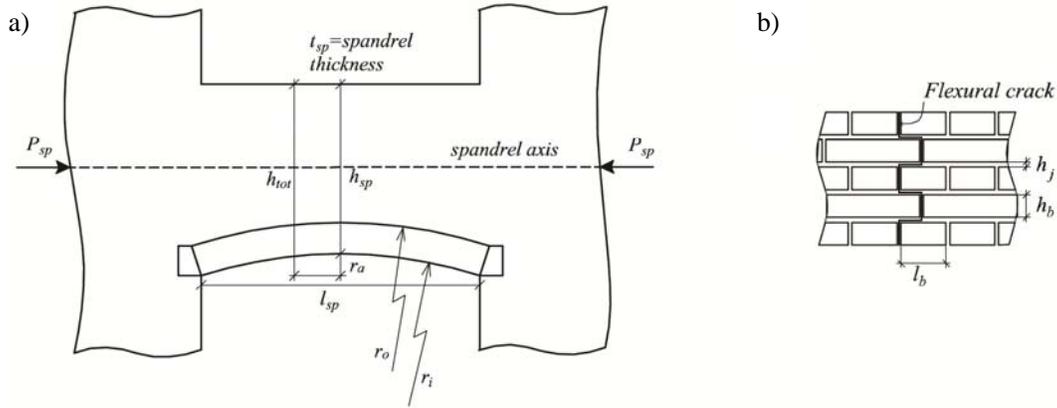
a)   b)

Figure 2. a. General geometry of spandrel; b. Geometry of bricks and mortar (Beyer, 2012)

3. EXPERIMENTAL STUDY

Beyer and Dazio (2012) tested four masonry spandrels that featured either a timber lintel or a shallow masonry arch. The results of one of the spandrel elements with a shallow arch were chosen to validate the numerical model. A brief summary of the experimental setup is given in the following section; for a more detailed description of the test see Beyer and Dazio (2012). The test consisted of quasi-static cyclic loading of masonry spandrels. A schematic diagram of the test setup is shown in Fig. 3. A drift was imposed on the two piers, which defined the deformation demand on the spandrel. The axial elongation of the spandrel was restrained by the horizontal rods. The axial force in the spandrel was kept constant throughout the test with the help of a special load control system. The mechanical

properties of the construction materials were determined by material tests which were carried along with the quasi-static cyclic tests. These properties are given in Fig. 3.
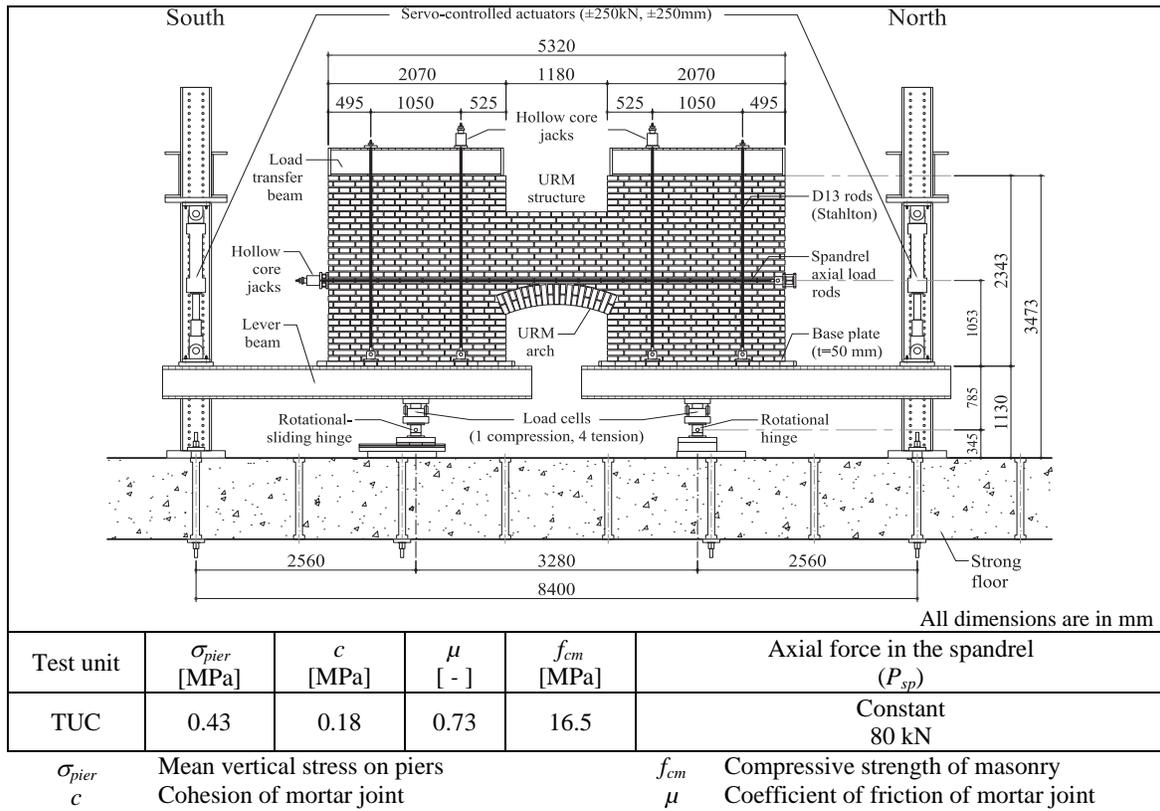

Test unit	σ_{pier} [MPa]	c [MPa]	μ [-]	f_{cm} [MPa]	Axial force in the spandrel (P_{sp})
TUC	0.43	0.18	0.73	16.5	Constant 80 kN

σ_{pier}	Mean vertical stress on piers		f_{cm}	Compressive strength of masonry
c	Cohesion of mortar joint		μ	Coefficient of friction of mortar joint

Figure 3. Test setup for spandrel test and mechanical properties of the constituent materials (Beyer and Dazio, 2012)

4. NUMERICAL MODELING OF MASONRY

A two-dimensional modeling approach was adopted in the current study to replicate the experimental test setup. The commercial finite element package ATENA (Cervenka, 2007) was used for the current study. Using the simplified micro-modeling approach each brick was modeled as a separate unit with contact properties assigned at the interface.
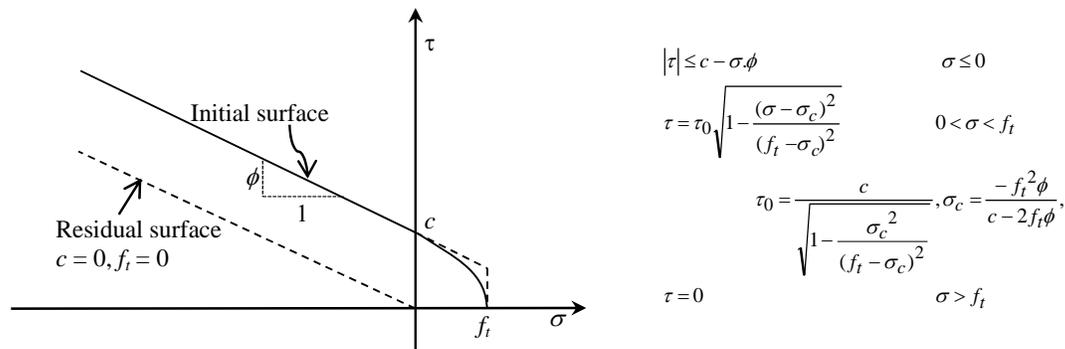

$$|\tau| \le c - \sigma.\phi \qquad \sigma \le 0$$

$$\tau = \tau_0 \sqrt{1 - \frac{(\sigma - \sigma_c)^2}{(f_t - \sigma_c)^2}} \qquad 0 < \sigma < f_t$$

$$\tau_0 = \frac{c}{\sqrt{1 - \frac{\sigma_c^2}{(f_t - \sigma_c)^2}}}, \sigma_c = \frac{-f_t^2 \phi}{c - 2f_t \phi},$$

$$\tau = 0 \qquad \sigma > f_t$$

Figure 4. Failure surface for interface elements

The interface was modeled according to the failure surface as shown in Fig. 4. The initial failure surface follows Mohr-Coulomb friction law with an ellipsoidal failure surface in the tension regime (Fig. 4). Once the interface reaches its maximum shear stress (τ), it loses its cohesion (c) and tensile strength (f_t). The residual failure surface accounts only for the frictional strength. The tensile and shear softening was defined based on the fracture energy associated with each mode.

4.1 Description of the model

The bricks were modeled as plane stress elastic isotropic elements with a mesh element size of 10 cm. The steel beams on the top and bottom of the masonry walls were also modeled as plane stress elastic isotropic elements with a mesh size of 10 cm. The meshes, both in the bricks and the steel beams, were of quadrilateral shape (CCISoQuad) and a mesh sensitivity study revealed that reducing mesh size further had no effect on the global response. The interface was modeled with 2D interface elements with the interface properties and the failure mechanism as given in Fig. 3 and 4. The tensile and shear softening of the interface was modeled based on the fracture energy associated with each mode and a linear variation was assumed in the current study. The fracture energy of the shear mode (G^{II}_f) was calculated from the experiments as 0.1 N/mm and the fracture energy (G^I_f) for the axial mode was assumed to be 1/10th of that for the shear mode, i.e., $G^I_f = 0.1\ G^{II}_f$.

a)   b)
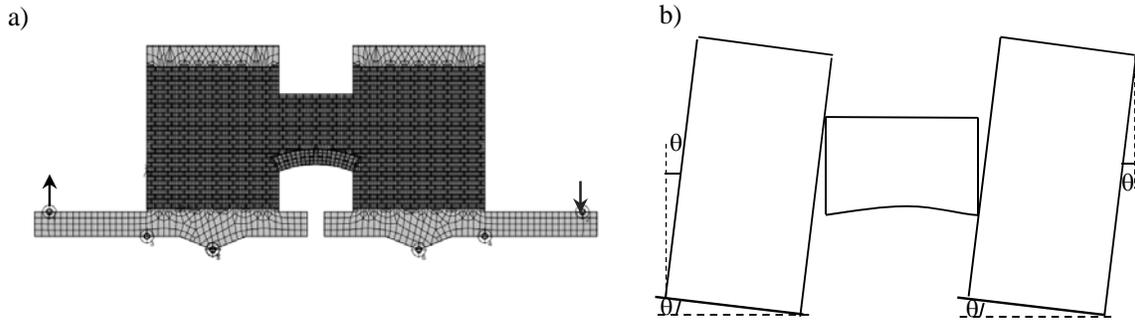

Figure 5. a. Numerical model for masonry-arch spandrel; b. Measurement of drift

A typical representation of the numerical model created in ATENA is shown in Fig. 5a. Although quasi-static cyclic loading was applied in the experiments of Beyer and Dazio (2012) the current numerical study is limited to monotonic loading, i.e., loading only in a single direction, for the following two reasons: (1) The envelope of the force deformation curve from the quasi static cyclic loading is an approximate representation of the force deformation curve from the monotonic loading. (2) As the objective of the current study is to conduct a parametric analysis, it is desirable to reduce the computational effort. The computational effort associated with monotonic loading is less in comparison to quasi-static cyclic loading.

The analysis of the numerical model was carried out in two steps. The axial loads on the piers and the spandrels were applied first, followed by the displacement at the end of the steel beams. The displacement was applied in the upward direction for the left steel beam and in the downward direction for the right steel beam (Fig. 5a). Numerical analysis was carried out with the standard Newton-Raphson algorithm. The tangent stiffness was updated at each step of the analysis. The number of iterations was restricted to 40 with a displacement error tolerance of 0.01. If the algorithm failed to converge the number of iterations was increased to 100.

4.2 Validation of the numerical model

The accuracy of the finite element model (FEM) was verified through the comparison with the experimental data for TUC from Beyer and Dazio (2012). The force-deformation behavior obtained from the numerical model and the experiments are shown in Fig. 6. The positive and negative envelope of the quasi-static cyclic loading from the experimental results is plotted in Fig. 6. The

numerical model is able to predict the peak strength as well as the force deformation characteristics up to a drift of 0.34 %, the maximum drift for which convergence was obtained. Figure 7 shows the deformed shape of the test unit and the numerical model at a drift of 0.2 %. The numerical model is able to capture the failure pattern with adequate accuracy.
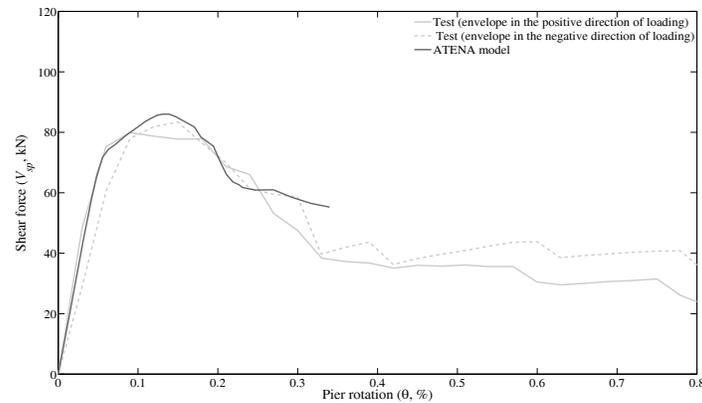

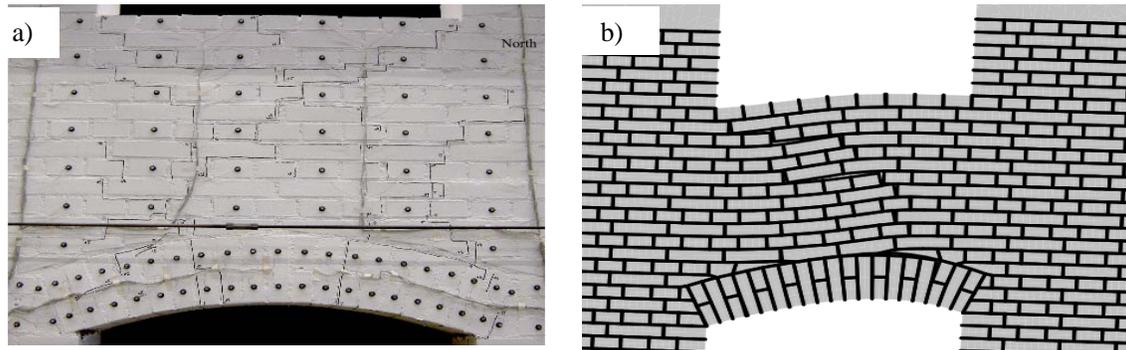**Figure 6.** Comparison of the numerical model with the experimental results

Figure 7. Deformed shape at a drift (θ) of 0.2 %, a. Test specimen TUC (Beyer and Dazio, 2012); b. Numerical model in ATENA (magnification factor of 10)

5. PARAMETRIC ANALYSIS AND COMPARISON WITH THE EXISTING MODELS

In order to identify the parameters that have a significant influence on the peak strength of the masonry spandrels, a parametric study was carried out by varying one parameter at a time from the numerical model used for experimental validation An initial sensitivity analysis revealed that the axial stress on the spandrel (p_{sp}), cohesion (c), and the ratio of the height of the spandrel to the length of the spandrel (h_{sp}/l_{sp}) are the most significant parameters that affect the peak strength and the mode of failure associated with masonry spandrels. A detailed parametric study was carried out to check the variation of the peak strength with respect to the parameters such as p_{sp}, c, and h_{sp}/l_{sp}. The results of the parametric studies are shown in Fig. 8 to 10. These figures also provide a comparison of the numerically determined peak strength values with those predicted by the existing mechanical models (section 2). The diagonal tensile strength of the masonry f_{dt} was not determined experimentally and a value of $f_{dt} = 0.10$ MPa was assumed for all spandrels. The horizontal strength f_{hd} of the masonry was also not determined experimentally and as a first approximation, f_{hd} was assumed to be equal to the vertical compressive strength of the masonry f_{cm} (Beyer and Dazio, 2012). The combined height of a brick and a joint was 74 mm. The length of a brick and the width of a head joint were assumed to be 120 mm and 10 mm, respectively.

5.1 The effect of axial stress on the peak strength of the spandrel

A parametric study was carried out using the model described in section 4 in order to ascertain whether the peak strength is affected by the axial stress in the spandrel. The axial stress was varied from 0 MPa to 0.25 MPa. The results of the parametric sensitivity analysis are shown in Fig. 8. Figure 8 shows that the peak strength of the spandrel is not much influenced by the axial stress on the spandrel, but determines the mode of failure associated with the masonry spandrel, i.e., flexural mode of failure is associated with low axial stresses and diagonal shear failure with higher axial stresses.
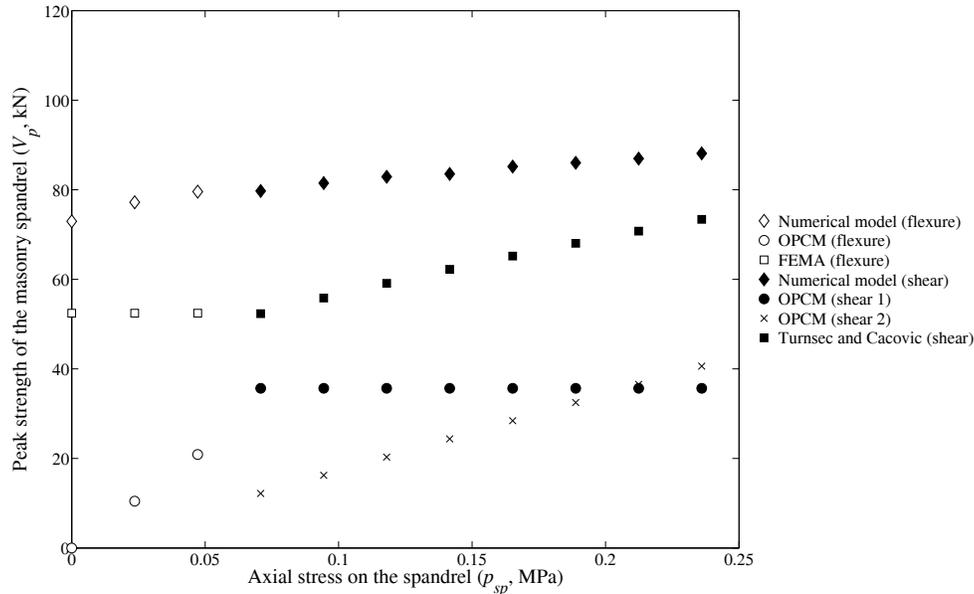

Figure 8. Variation of peak strength with respect to the change in the axial stress on the spandrel

Figure 8 shows that none of the existing models are able to predict the peak strength of the masonry spandrels. OPCM models significantly underestimate the peak strength of the masonry spandrels. Although the Turnsek and Cacovic model significantly underestimate the peak strength of the masonry spandrels, it is the only model which can provide a fair estimate of the peak strength of the masonry spandrels. It is, however, to be noted that the current comparison by Turnsek and Cacovic model is based on an assumed diagonal tensile strength. The FEMA flexural model predicts a constant peak strength when the axial load is varied. This is expected since the influence of the axial load was not considered in the FEMA model

5.2 The effect of cohesion on the peak strength of the spandrel

In order to study the effect of cohesion (c) on the peak strength of the spandrel, a parametric study was conducted for various values of cohesion (ranging from 0.10 MPa to 0.30 MPa). The diagonal shear mode was observed to be the failure mode for the selected spandrels. The variation of the peak strength with respect to the change in cohesion is shown in Fig. 9a. Figure 9a shows that the peak strength is greatly affected by cohesion and increases with an increase in cohesion. The OPCM model (shear 2) and the Turnsek and Cacovic model predict constant peak strength irrespective of the value of cohesion. The model by OPCM (shear 1) is able to identify the trend in the variation of peak strength with respect to the change in the cohesion, albeit with a constant offset.
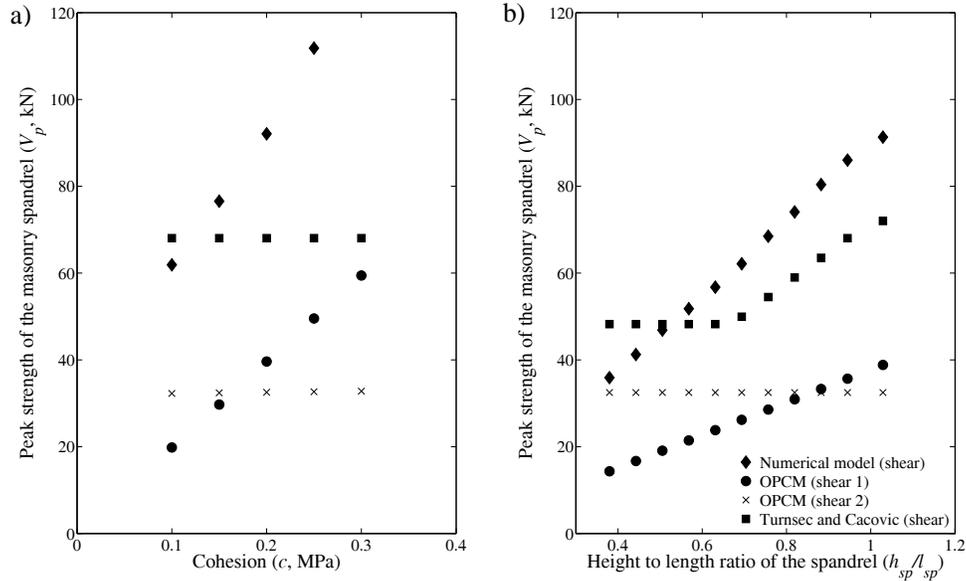
Figure 9. Variation of peak strength with respect to, a. Change in cohesion; b. Height to length ratio of the spandrel

5.3. The effect of height to length ratio of the spandrel on the peak strength of the spandrel

Figure 9b shows the results of a parametric study on the influence of the ratio h_{sp}/l_{sp} on the peak strength of the masonry spandrel. The load-carrying capacity diminishes as the pier becomes more and more slender. OPCM model (shear 2) is unable to capture the variation of the peak strength with respect to the h_{sp}/l_{sp} ratio although they are able to predict the peak strength values at low slenderness ratios. The Turnsek and Cacovic shear model can identify the variation of the peak shear strength with respect to the change in the h_{sp}/l_{sp} ratio.
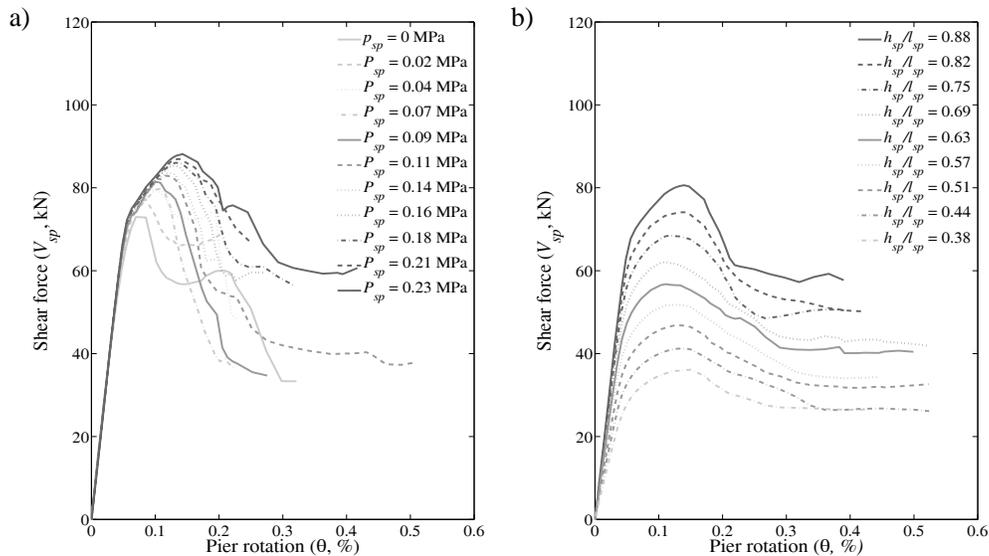

Figure 10. Force-deformation characteristics of the masonry spandrel with respect to a) change in axial stress on the spandrel; b) height to length ratio of spandrel

6. FORCE-DEFORMATION CHARACTERISTICS OF MASONRY SPANDRELS

The force-deformation characteristics of the masonry spandrel for different axial stresses (p_{sp}) and height to length ratio of spandrel (h_{sp}/l_{sp}) are shown in Fig. 10. The shear force in the spandrel varies linearly with the rotation (θ) up to a point where the first cracks form in the spandrel, similar to what was noticed from the experiments (Beyer and Dazio, 2012). The stiffness of the spandrel reduces once it cracks, but the shear carrying capacity increases till the peak strength is reached. The shear strength capacity reduces rapidly beyond the peak strength.

7. CONCLUSIONS

In spite of the importance of masonry spandrels in the force-deformation characteristics of masonry piers, they are rarely considered in designs due to the lack of experimental data and mechanical models. A detailed parametric study was carried out to identify the parameters that have a significant influence on the peak strength of the masonry spandrels with shallow arches. Parametric studies revealed that the cohesion (c) and the height to length ratio of the spandrel (h_{sp}/l_{sp}) are the most sensitive parameters affecting the peak strength of masonry spandrels. The mode of failure (flexure or diagonal shear) of the masonry spandrels is determined by the axial stress in the spandrel.

The current study shows that the existing models (FEMA and OPCM) significantly underestimate the peak strength of masonry spandrels. The peak strength capacity of the spandrel might be of interest for the assessment of a building before an earthquake when a visual inspection has shown that the spandrels are still largely uncracked and the few existing cracks are small. Future work should therefore expand the existing mechanical models of masonry spandrels such that they can capture the variation of the peak strength with respect to cohesion and height to length ratio of the spandrel. The current study focuses only on the peak strength of the masonry spandrel with shallow arches; residual strength, limit rotations are not addressed and are the subject of ongoing studies.

REFERENCES

ATC (1998) FEMA–306. Evaluation of earthquake damaged concrete and masonry wall buildings. *Basic Procedures Manual, Applied Technology Council,* Washington DC, United States.

Beyer, K. and Dazio, A. (2011). Modeling of spandrel elements in URM structure with RC slabs or ring beams. *Proceedings of the Eleventh North American Masonry Conference*, Minneapolis, United States. 3.02-5.

Beyer, K. and Dazio, A. (2012). Quasi-static cyclic tests on masonry spandrels. Accepted for publication in Earthquake Spectra (article available on http://eesd.epfl.ch/page-18604-en.html).

Beyer, K. and Mangalathu, S. (2012). Review of strength models for masonry spandrels. Communicated to Bulletin of Earthquake Engineering.

Beyer, K. (2012). Peak and residual strength of masonry spandrels. Accepted for publication in Engineering Structures, **41**, 533-547.

Carvenka, V. (2007). Atena–Computer program for nonlinear finite element analysis of reinforced concrete structures. *Theory and User Manual*, Prague, Czech Republic.

Gambarotta, L. and Lagomarsino, S. (1997). Damage models for the seismic response of brick masonry shear walls, Part II: The continuum model and its applications. *Earthquake Engineering and Structural Dynamics,* **26:4**, 441-462.

Gattesco, N., Clemente, I., Macorini, L. and Noe, S. (2008). Experimental investigation of the behavior of spandrels in ancient masonry buildings. *Proceedings of the 14th world conference on earthquake engineering*, October 12-17, 2008. Beijing, China, 511-046.

Lourenco, P. B. (1994). Analysis of masonry structures with interface elements–theory and applications. *TU Delft report no. 03-21-22-0-91*, Technical University Delft, The Netherlands.

Magenes, G. (2000). A method for pushover analysis in seismic assessment of masonry buildings. *Proceedings of the 12th world conference on earthquake engineering*, January 30-February 4, 2000. Auckland, New Zealand, No. 1866.

O.P.C.M 3274, 20/03/2003 Primi elementi in materia di criteri generali per la classificazione sismica del territorio nazionale e di normative tecniche per le costruzioni in zona sismica (in Italian).

O.P.C.M 3431/05, 09/05/2005 Ulteriori modifiche ed integrazioni all OPCM 3274/03 (in Italian).

Turnsek, V. and Cacovic, F. (1970). Some experimental results on the strength of brick masonry walls. *Proceedings of the 2nd international brick masonry conference*, Stoke on Trent, United Kingdom, 149-156.